Transient Analysis of Full-Wave Generalized PEEC Model for Interconnection Problems

Yuhang Dou, *Student Member, IEEE*, and Ke-Li Wu, *Fellow, IEEE*

***Abstract*— In this article, an efficient transient analysis method for high-speed interconnection and packaging problems is proposed. The method is committed to a full-wave generalized partial element equivalent circuit (G-PEEC) model with guaranteed stability and causality. With the proposed method, the full-wave G-PEEC model is represented by a few static compact subcircuits that are derived by applying the micromodeling circuit method to the G-PEEC model at a few discrete frequency points. Its transient response can be obtained by a linear combination of responses of the compact subcircuits, which can be simulated by the transient analysis method of SPICE. By adopting the compact subcircuits, which is an order reduced G-PEEC model, the transient simulation can be speeded up by two orders of magnitude when compared with the case if the subcircuits are generated directly from the G-PEEC model. Since the compact subcircuits are static, physically meaningful, and passive, the proposed transient analysis is with guaranteed stability and causality. Moreover, a frequency compensation strategy is proposed for preparing input signals of subcircuits to avoid the Gibbs phenomenon. Finally, three numerical examples, including eye-diagrams for a practical multilayer interconnection problem, are given, demonstrating the effectiveness, accuracy, scalability, and simplicity of the proposed method.**

***Index Terms*— Causality, electromagnetic (EM), frequency-dependent elements, passivity, signal integrity (SI), stability, transient analysis.**

I. Introduction

As THE demand for high data rate and compact electronics systems increases, the density of circuit board layout and the complexity of the packaging and interconnection circuits continuously increase. As such, the dispersion effects, including the parasitic radiation and frequency dependence of the circuit components that were conventionally approximated by a static circuit model, have to be brought into design considerations. Therefore, a full-wave model is needed to accurately describe the ever-increasing complex full-wave electromagnetic (EM) phenomena presented in high-speed circuit structures for an accurate understanding of signal integrity (SI) characteristics. In this regard, a stable, causal, accurate, and efficient transient analysis method, which is suitable for a full-wave circuit model, would be highly desirable to the industry.

Manuscript received November 5, 2018; revised May 2, 2019; accepted July 6, 2019. Date of publication September 4, 2019; date of current version October 4, 2019. This work was supported by the University Grants Committee of Hong Kong under Grant AoE/P-04/08. *(Corresponding author: Ke-Li Wu.)*

The authors are with the Department of Electronic Engineering, The Chinese University of Hong Kong, Hong Kong (e-mail: yhdou@link.cuhk.edu.hk; klwu@cuhk.edu.hk).

Color versions of one or more of the figures in this article are available online at http://ieeexplore.ieee.org.

Digital Object Identifier 10.1109/TMTT.2019.2934448

Traditionally, a time-domain response of a full-wave model relies on the convolution-based methods, by which the time-domain response for a given input signal is obtained by convolution of the input signal with the impulse response of the system if it can be reliably available. There are two categories of the convolution-based analysis methods: the numerical convolution-based methods [1]–[11] and the recursive convolution-based methods [12]–[18]. The numerical one generates a numerical impulse response from the frequency-domain response using the inverse fast Fourier transformation (IFFT) [2], [3]. Such methods require massive samples of the frequency-domain response, which may be expensive to obtain through EM simulation. Due to the limited bandwidth of the frequency-domain response, the direct IFFT may violate the causality, thereby resulting in inaccurate SI quantities [19], [20]. To tackle this problem, many causality enforcement approaches were proposed [5]–[10]. Such approaches may need to alter the original frequency response to retain the fidelity to a certain extent [21]. Moreover, the Gibbs phenomena and aliasing errors caused by the band-limited frequency-domain response and input signal will be accumulated, leading to the instability problem [11].

On the contrary, the recursive convolution-based method approximates the frequency-domain response as a rational function, such as the vector fitting method [12]–[15] or the asymptotic waveform evaluation (AWE) method [16]–[18]. Then the impulse response in time-domain can be derived from the approximated rational function, which is in the form of a sum of exponentials. The vector fitting method also needs the response in a sufficiently wide frequency band to include a sufficient number of system poles [22]. Meanwhile, the AWE method derives a rational model from the state-space matrices [16]. The method may not be suitable for a full-wave EM problem because the state-space matrices obtained from a full-wave circuit model are frequency-dependent. In addition, the passivity of these rational models cannot be assured, even when the system is stable [4], [23].

In this article, an efficient transient analysis method for high-speed interconnection and packaging problems is proposed. The method is committed to a full-wave generalized partial element equivalent circuit (G-PEEC) model, in which full-wave EM effects have been accurately reflected by self- and mutual inductances, capacitances, and radiation resistances [24]–[26]. With the proposed transient analysis method, the full-wave G-PEEC model can be represented by a few static and passive compact subcircuits that are obtained by applying the micromodeling method at discrete

frequencies [27]–[29]. The most attractive feature of the proposed method is that it turns a transient response problem of the full-wave G-PEEC model into a few numbers of transient analysis problems of static and passive subcircuits, which can be computed independently by a traditional transient analysis tool, such as a SPICE-like circuit solver with guaranteed stability and causality [30], [31]. Obtaining the transient response of the full-wave G-PEEC model becomes a linear combination of those of the subcircuits. Therefore, unlike the convolution-based methods, which heavily rely on the quality of the frequency-domain response and require mathematics-involved causality and passivity enforcement processes, the proposed method executes the transient analysis of a few static and passive subcircuits efficiently.

Although an earlier conference article [32] reported some preliminary results of the concept using direct subcircuits generated directly from the G-PEEC model, four important aspects that ensure a stable, causal, and accurate transient response of a full-wave G-PEEC model are addressed in this work: 1) adopting the micromodeling circuit method for generating passive compact subcircuits; 2) finding an optimal sampling strategy for obtaining the subcircuits from a full-wave G-PEEC model; 3) eliminating the Gibbs phenomenon in the transient analysis by introducing a compensation scheme in preparing input signals of subcircuits; and 4) approximating the frequency response as a continuous function.

Overall, the proposed method exhibits the following unique advantages.

1) The transient analysis can be accelerated by two orders of magnitude using the micromodeling circuit method.
2) The obtained transient response is guaranteed to be stable and causal.
3) The method eliminates the Gibbs phenomenon and aliasing problem.
4) A high computational efficiency in the transient analysis because only one matrix inversion is involved in the transient analysis of each subcircuit if a constant time interval is used.

A brief review of the transient analysis method and the recently developed passive micromodeling circuit method are given in Sections II and III, respectively. Then, the complete theory of the proposed method is described systematically in Section IV, followed by three numerical examples in Section V, demonstrating its fidelity, efficiency, scalability, and simplicity. The proposed method is suitable for EM problems with multilayer frequency-independent dielectrics and problems with external linear components.

II. Transient Analysis Method

The uniqueness of the proposed transient analysis for a full-wave G-PEEC model is to break down a complex transient analysis problem into a few transient analysis problems of the static and passive compact subcircuits. For convenience, the modified nodal analysis (MNA) for the transient analysis [30] is briefly reviewed.

The transient analysis method generates the time-domain response by solving the differential-algebraic equations, which can be obtained directly from a static *RLC* circuit, such that

$$\mathbf{E}\dot{\mathbf{x}}(t) = \mathbf{A}\mathbf{x}(t) + \mathbf{B}\mathbf{u}(t) \tag{1a}$$

$$\mathbf{y}(t) = \mathbf{C}^T\mathbf{x}(t) + \mathbf{D}\mathbf{u}(t) \tag{1b}$$

where the *dot* above $\mathbf{x}$ denotes time derivative, and the number of ports and the dynamic order are denoted by p and q, respectively. The state vector $\mathbf{x} \in \mathbf{R}^q$ includes the internal node voltages and branch currents, $\mathbf{u} \in \mathbf{R}^p$ is the input vector, $\mathbf{y} \in \mathbf{R}^p$ is the output vector, and $\mathbf{A} \in \mathbf{R}^{q\times q}$, $\mathbf{B} \in \mathbf{R}^{q\times p}$, $\mathbf{C} \in \mathbf{R}^{p\times q}$, $\mathbf{D} \in \mathbf{R}^{p\times p}$, and $\mathbf{E} \in \mathbf{R}^{p\times p}$ are the static space matrices.

To solve the differential-algebraic equations (1), they are approximated into a finite-difference form

$$\dot{\mathbf{x}}_n = (\mathbf{E} - 0.5h\mathbf{A})^{-1}\left(\mathbf{A}\mathbf{x}_{n-1} + 0.5h\mathbf{A}\dot{\mathbf{x}}_{n-1} + \mathbf{B}\mathbf{u}_n\right) \tag{2a}$$

$$\mathbf{y}_n = \mathbf{C}^T\mathbf{x}_n + \mathbf{D}\mathbf{u}_n \tag{2b}$$

using the trapezoidal rule

$$\mathbf{x}_n = \mathbf{x}_{n-1} + 0.5h\left(\dot{\mathbf{x}}_n + \dot{\mathbf{x}}_{n-1}\right). \tag{3}$$

The subscript n represents the nth time-step and the constant h is the time interval between two time-steps. The trapezoidal rule is acquiescently accepted in the SPICE software package because it can provide good numerical stability when the system is passive, regardless of the time-step h [31]. Therefore, the output of a passive subcircuit obtained by the transient analysis method is guaranteed to be stable.

Causality is another crucial property of a transient analysis. The output is causal if the output at time $t = t_0$ does not depend on the value of the input for times $t > t_0$ [33]. Because (2) indicates that the output $\mathbf{y}_n$ at the nth time-step depends only on the signal $\mathbf{x}_{n-1}$, $\dot{\mathbf{x}}_{n-1}$, and $\mathbf{u}_n$ at the time-steps not larger than n, the output response generated by the transient analysis method must be causal.

To obtain the output $\mathbf{y}_n$, as suggested by (2a), the matrix inversion of $(\mathbf{E} - 0.5h\mathbf{A})$ is needed. If the transient analysis uses constant time interval h, the matrix $(\mathbf{E} - 0.5h\mathbf{A})$ is the same at every time-step and only one matrix inversion is needed. Therefore, the matrix multiplication in (2a) is the dominant computational overhead with the complexity of $O(N^2)$.

III. Micromodeling Circuit Method

The micromodeling circuit method used in this article refers to the systematic method that converts a multiconductor EM problem into a compact passive *RLC* circuit model proposed recently [27]–[29], which is an order-reduced version of the G-PEEC model. In the G-PEEC model as shown in Fig. 1, the self- or mutual radiation resistances and self- or mutual inductances are frequency-dependent, but the self- or mutual capacitances are frequency-independent. There are four major reasons to use the micromodeling circuit method to generate static compact subcircuits.

1) It reduces the order of the original G-PEEC model by one order of magnitude, which leads to an acceleration of transient simulation by two orders of magnitude.
2) It generates a required static and passive subcircuit.
3) It does not suffer from any scalability issues as no matrix inversions or decompositions are involved in its derivation process.

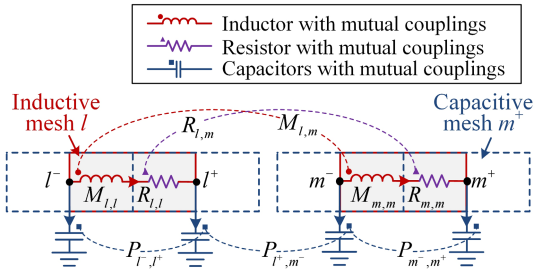

Fig. 1. Representative circuit topology of the G-PEEC model.

4) Its derivation is highly suitable to be speeded up using GPU parallel computation technique [34], [35].

IV. Transient Analysis of a Full-Wave Circuit

The proposed transient analysis method starts from approximating the full-wave G-PEEC model by a few static and passive compact subcircuits that are obtained by the micromodeling circuit method at a few frequency points. It will be shown that the time-domain response of the full-wave G-PEEC model can be expressed as a linear combination of the time-domain responses of the compact subcircuits.

A. Approximation of Frequency Response

For a full-wave circuit model, its frequency response can be denoted as $H(\omega, E(\omega))$, where ω represents the working angular frequency, and $E(\omega)$ indicates that the circuit elements are the functions of ω. The frequency response of the full-wave large-scale circuit can be approximated accurately by several compact static subcircuits using the following strategy.

For an SI analysis, the frequency band of interest is low-pass in nature with cutoff frequency ω_{Max}. In Fourier analysis, the whole frequency band $[-\infty, +\infty]$ is divided into N subfrequency bands at frequency points $\omega_1, \omega_2, \ldots, \omega_N$, where $\omega_1 = 0$ and $\omega_N = \omega_{\text{Max}}$. In the N subfrequency bands, N static subcircuits are generated at frequency $\omega_1, \omega_2, \ldots, \omega_N$. In a previous work [32], subcircuits are directly obtained by sampling the full-wave G-PEEC model, which are called direct subcircuits. However, the compact subcircuits obtained by the micromodeling method are used in the proposed method to accelerate the transient simulation. In the ith subfrequency band $[-\omega_{i+1}, -\omega_i] \cup [\omega_i, \omega_{i+1}]$, the variation in the circuit elements versus frequency of the original full-wave G-PEEC model is assumed to be negligible in [32]. The original frequency response $H[\omega, E(\omega)]$ in the ith subfrequency band is roughly approximated by $H[\omega, E(\omega_i)]$ of the ith direct subcircuit, which is not continuous at the frequency band boundaries. To acquire a continuous frequency response and improve approximation accuracy, the frequency response $H[\omega, E(\omega)]$ in the ith bands of $[-\omega_{i+1}, -\omega_i] \cup [\omega_i, \omega_{i+1}]$ is proposed to be approximated by the linear combination of frequency responses of the ith and $(i+1)$th compact subcircuits as

$$H(\omega, E(\omega)) \approx w_i(\omega) H(\omega, E(\omega_i)) + w_{i+1}(\omega) H(\omega, E(\omega_{i+1})), \quad \text{for } \omega \in [-\omega_{i+1}, -\omega_i] \cup [\omega_i, \omega_{i+1}], \tag{4}$$

where $w_i(\omega)$ and $w_{i+1}(\omega)$ are the continuous window functions of the ith and the $(i+1)$th subcircuits, respectively. The window functions can be determined by the user, which will be introduced in Section IV-D. The window functions need to follow the constraint $w_i(\omega)$ equals to zero outside of the $(i-1)$th and ith subfrequency bands $[-\omega_{i+1}, -\omega_{i-1}] \cup [\omega_{i-1}, \omega_{i+1}]$. And the sum of $w_i(\omega)$ and $w_{i+1}(\omega)$ is 1 in the ith subfrequency band $[-\omega_{i+1}, -\omega_i] \cup [\omega_i, \omega_{i+1}]$.

The influence of the frequency response in the Nth subfrequency band $[-\infty, -\omega_N] \cup [\omega_N, +\infty]$ is not taken into account in [32] and other convolution-based methods. This omission will cause a serious Gibbs phenomenon in the transient analysis.

To address the aforementioned issues, the frequency response of a full-wave G-PEEC model in the Nth subfrequency band can be approximated by $H[\omega, E(\omega_N)]$, which is the frequency response of the Nth subcircuit with circuit elements sampled at ω_N. Although the approximation is a bit rough in the Nth subfrequency band, it can relieve the Gibbs phenomenon and sacrifice the accuracy very little because the input signal components in the Nth subfrequency band are minor.

In summary, with a legitimate subfrequency band assignment and appropriate window functions $w_i(\omega)$, the frequency response of a full-wave G-PEEC model can be accurately approximated according to (4) as

$$\begin{aligned} H(\omega, E(\omega)) &\approx \sum_{i=1}^{N-1} [w_i(\omega) H(\omega, E(\omega_i)) + w_{i+1}(\omega) H(\omega, E(\omega_{i+1}))] \\ &\quad \times [u(\omega - \omega_i) - u(\omega - \omega_{i+1}) + u(\omega + \omega_{i+1}) - u(\omega + \omega_i)] \\ &\quad + w_N(\omega) H(\omega, E(\omega_N)) [u(\omega - \omega_N) - u(\omega + \omega_N) + 1] \end{aligned} \tag{5}$$

where $u(\omega)$ is the unit-step function. The last term of (5) interprets the approximated frequency response of the system in the Nth subfrequency band $[-\infty, -\omega_N] \cup [\omega_N, +\infty]$, which compensates the missing information of the frequency response when the response is approximated only by the first $(N-1)$ subcircuits in the limited frequency band $[-\omega_N, \omega_N]$ as suggested in [32].

B. Transient Response of a Full-Wave Circuit Model

Having had the approximation of the frequency response $H[\omega, E(\omega)]$ by the linear combination of the frequency responses of N static compact subcircuits, it will be straightforward to obtain the output response $Y(\omega)$ with respect to a given input signal $X(\omega)$ in the frequency-domain by

$$\begin{aligned} Y(\omega) &= H(\omega, E(\omega)) X(\omega) \\ &\approx H(\omega, E(\omega_1)) X(\omega) w_1(\omega) \\ &\quad \times [u(\omega - \omega_1) - u(\omega - \omega_2) + u(\omega + \omega_2) - u(\omega + \omega_1)] \\ &\quad + \sum_{i=2}^{N-1} H(\omega, E(\omega_i)) w_i(\omega) X(\omega) \\ &\quad \times [u(\omega - \omega_{i-1}) - u(\omega - \omega_{i+1}) + u(\omega + \omega_{i+1}) \\ &\quad - u(\omega + \omega_{i-1})] \end{aligned}$$

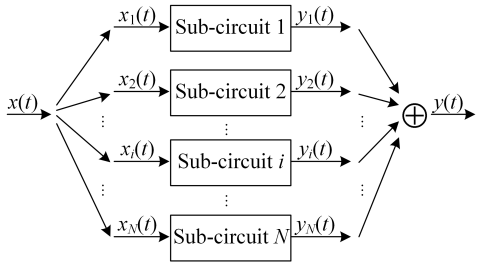

Fig. 2. Illustration of the proposed simulation scheme: computation of time-domain response $y(t)$ of a full-wave circuit model for input $x(t)$ can be performed by a linear combination of transient responses of several static passive subcircuits.

$$+ H(\omega, E(\omega_N))X(\omega)w_N(\omega) \times [u(\omega-\omega_N)-u(\omega+\omega_N)+1] = \sum_{i=1}^{N} H(\omega, E(\omega_i))X_i(\omega) \quad (6)$$

where $Y(\omega)$ and $X(\omega)$ are the Fourier transformations of the output signal $y(t)$ and the input signal $x(t)$, respectively. Equation (6) suggests that one can define the input signal $X_i(\omega)$ of the ith subcircuit in the frequency-domain as

$$X_i(\omega) = \begin{cases} X(\omega)w_1(\omega)[u(\omega-\omega_1)-u(\omega-\omega_2) \\ \qquad +u(\omega+\omega_2)-u(\omega+\omega_1)], & i=1 \\ X(\omega)w_i(\omega)[u(\omega-\omega_{i-1})-u(\omega-\omega_{i+1}) \\ \qquad +u(\omega+\omega_{i+1})-u(\omega+\omega_{i-1})], & 1<i<N \\ X(\omega)w_N(\omega)[u(\omega-\omega_N)-u(\omega+\omega_N)+1], & i=N. \end{cases} \quad (7)$$

Theoretically, the time-domain response can be obtained by invert Fourier transformation of (6) as

$$y(t) = \mathcal{F}^{-1}[Y(\omega)] \approx \mathcal{F}^{-1}\left[\sum_{i=1}^{N} H(\omega, E(\omega_i))X_i(\omega)\right] = \sum_{i=1}^{N} \mathcal{F}^{-1}[H(\omega, E(\omega_i))] * x_i(t). \quad (8)$$

The uniqueness of the proposed method is that $y_i(t)$ can be directly simulated by the transient analysis of the ith static passive subcircuit model. Free of calculating the output response $y_i(t)$ of the ith static subcircuit by convolution of $\mathcal{F}^{-1}[H(\omega, E(\omega_i))] * x_i(t)$ in the frequency-domain can avoid the instability and noncausality problems and can use the $x_N(t)$ in Nth subfrequency band $[-\infty, -\omega_N] \cup [\omega_N, +\infty]$ to relieve the Gibbs phenomenon.

In summary, (8) proves that the transient analysis for a full-wave circuit model can be decomposed into the transient analysis problems of several static passive subcircuits. Fig. 2 illustrates this process.

C. Preparation of Compact Subcircuits

The accuracy of the proposed method is subject to the sampling strategy of the full-wave G-PEEC model for preparing the compact subcircuits. Increasing the maximum sampling frequency and decreasing the frequency interval of the subcircuits improve the accuracy but with the cost of increasing the computational overhead. Therefore, a legitimate sampling strategy is needed to ensure an optimal number of compact subcircuits with a preset accuracy criterion.

To develop an optimal sampling strategy, there are two aspects that must be taken into account: 1) determining the maximum sampling frequency ω_{Max} and 2) choosing the sampling frequencies for creating compact subcircuits.

1) Determination of ω_{Max}: When the spectral components of the input signal $X(\omega)$ outside the frequency band $[-\omega_{\text{Max}}, \omega_{\text{Max}}]$ approach zero, the output response $Y(\omega)$ is dominantly affected by the properties of the frequency response $H[\omega, E(\omega)]$ within the frequency band. Therefore, the maximum sampling frequency of subcircuits can be determined by the allowed energy of $X(\omega)$ falling outside of $[-\omega_{\text{Max}}, \omega_{\text{Max}}]$.

Usually, the input signal for an SI analysis is a pulse sequence, such as the pseudorandom binary sequence (PRBS) for the eye-diagram simulation. For example, take a single pulse signal with pulsewidth τ as an example. It has been shown that 97.88% of the total energy is distributed in the frequency band of $[-5\Omega_S, 5\Omega_S]$, where $\Omega_S = 2\pi/\tau$[36]. For an arbitrary pulse sequence signal, its spectrum is a linear combination of the spectrum of a single pulse signal. As a result, the majority of the energy of an arbitrary pulse sequence is distributed in the frequency band of $[-5\Omega_S, 5\Omega_S]$. And $5\Omega_S$ can be used as the maximum sampling frequency. In other words, $\omega_{\text{Max}} = 10\pi/\tau$.

2) Determination of Optimal Sampling Frequencies: The proposed method uses static passive subcircuits defined in its subfrequency bands. To ensure the accuracy of the approximation, the variation in the circuit elements versus frequency of the full-wave circuit in a subfrequency band needs to be smaller than a preset criterion δ_c. Therefore, the sampling frequencies of subcircuits are determined by an allowed maximum element variation.

To create the static compact subcircuits, the passive micromodeling method developed in [28] is applied to the full-wave G-PEEC model. It can be found in [28, eq. (23)] that the frequency dependence of circuit elements in a micromodeling circuit is dictated by three coefficients, namely, c_1, c_2, and c_3 with the following relation:

$$c_1 = \omega^2(m_{SS}+m_{II}-2m_{SI})/(p_{SS}+p_{II}-2p_{SI}) \quad (9a)$$

$$c_2 = \omega^2(m_{II}-m_{SI})/(p_{II}-p_{SI}) \quad (9b)$$

$$c_3 = \omega^2(m_{SS}-m_{SI})/(p_{SS}-p_{SI}) \quad (9c)$$

where m_{SS}, m_{II}, m_{SI}, p_{SS}, p_{II}, and p_{SI} are the known inductances and potances (coefficients of potential) related to an absorbed node, respectively. The maximum variation in c_1, c_2, and c_3 of the micromodeling circuit occurs when absorbing the last node at the end of the micromodeling circuit process. The maximum variation indicates the variation in the subcircuit elements in a subfrequency band. Define the largest frequency dependence coefficient $C(\omega)$ in a subcircuit as

$$C(\omega) = \omega^2 \max\left(\frac{m_{SS}+m_{II}-2m_{SI}}{p_{SS}+p_{II}-2p_{SI}}, \frac{m_{II}-m_{SI}}{p_{II}-p_{SI}}, \frac{m_{SS}-m_{SI}}{p_{SS}-p_{SI}}\right) = \omega^2 c_{\max}. \quad (10)$$

Because $C(\omega)$ is a monotonic function of frequency, the ripple bound δ of circuit elements of the subcircuit for the ith subfrequency band $[-\omega_{i+1}, -\omega_i] \cup [\omega_i, \omega_{i+1}]$ can be found as

$$\delta = \left(\omega_{i+1}^2 - \omega_i^2\right) c_{\max}. \tag{11}$$

For a preset upper bound of the ripple, δ_c, sampling frequencies in the frequency band $[0, \omega_{\text{Max}}]$ can be obtained in the ascending order. When the ith sampling frequency ω_i is determined, the $(i+1)$th sampling frequency ω_{i+1} should satisfy that

$$\omega_{i+1} \le \sqrt{\omega_i^2 + \delta_c / c_{\max}}. \tag{12}$$

According to (12), the bandwidth for the subcircuits can be optimally chosen and is not uniform.

D. Preparation Input Signals of Subcircuits

According to (7) and (8), preparing the input signal $x_i(t)$ for subcircuit 1 to $N-1$ involves four steps: 1) obtaining the Fourier transformation $X(\omega)$ of the original input signal $x(t)$ in the frequency band $[0, \omega_{\text{Max}}]$ using the discrete Fourier transform, 2) choosing an appropriate window function $w_i(\omega)$, 3) determining input signal $X_i(\omega)$ for the ith subcircuit using (7), and 4) generating $x_i(t)$ in the time-domain from $X_i(\omega)$ through discrete inverse Fourier transform.

Therefore, the time-domain input signal for subcircuit i $(i = 1, \ldots, N-1)$ can be obtained as

$$\begin{aligned} x_i(t) &= F^{-1}[X_i(\omega)] \\ &= \frac{1}{2\pi}\left[\int_{\omega_{i-1}}^{\omega_{i+1}} X(\omega) w_i(\omega) e^{j\omega t} d\omega \right. \\ &\qquad \left. + \int_{-\omega_{i+1}}^{-\omega_{i-1}} X(\omega) w_i(\omega) e^{j\omega t} d\omega\right] \\ &= \frac{1}{\pi}\int_{\omega_{i-1}}^{\omega_{i+1}} w_i(\omega) Re[X(\omega) e^{j\omega t}] d\omega, \\ &\quad i = 1, \ldots, N-1 \end{aligned} \tag{13}$$

in which the relation $X(-\omega) = X^*(\omega)$ is used. To calculate the input signal of subcircuits numerically, only the discrete values of $X(\omega)$ are needed, which can be obtained easily using the discrete Fourier transformation of the original input signal.

The input signal $x_N(t)$ for the Nth subcircuit cannot be obtained by the same token because of its infinite bandwidth. The infinite bandwidth is also the bottleneck of the convolution-based methods. In the time-domain, input signal $x_N(t)$ for the Nth subcircuit is found easily as

$$x_N(t) = x(t) - \sum_{i=1}^{N-1} x_i(t) \tag{14}$$

which compensates not only the missing contribution of the frequency response in the Nth subfrequency band $[-\infty, -\omega_N] \in [\omega_N, +\infty]$ in [32] but also the numerical error in generating the input signals for subcircuits 1 to $N-1$. Introducing $x_N(t)$ can significantly alleviate the Gibbs phenomenon in the transient analysis and highly preserve the fidelity of the input signal in the overall time-domain analysis.

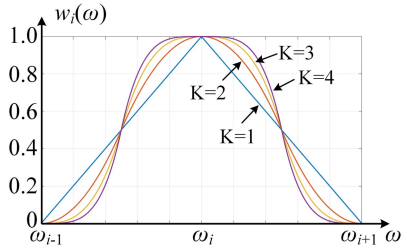

Fig. 3. Window function for the ith subcircuit with different parameter K.

The window function $w_i(\omega)$ in (5), (7), and (13) is introduced to ensure the continuity of the frequency response and to enhance the accuracy. The following piecewise window function is used in this work

$$w_1(\omega) = \begin{cases} 1 - \dfrac{1}{2}\left(2\dfrac{\omega-\omega_1}{\omega_2-\omega_1}\right)^K, & \omega_1 \le \omega \le \dfrac{\omega_1+\omega_2}{2} \\ \dfrac{1}{2}\left(2\dfrac{\omega-\omega_2}{\omega_1-\omega_2}\right)^K, & \dfrac{\omega_1+\omega_2}{2} \le \omega \le \omega_2 \end{cases} \tag{15a}$$

$$w_i(\omega) = \begin{cases} \dfrac{1}{2}\left(2\dfrac{\omega-\omega_{i-1}}{\omega_i-\omega_{i-1}}\right)^K, & \omega_{i-1} \le \omega \le \dfrac{\omega_{i-1}+\omega_i}{2} \\ 1 - \dfrac{1}{2}\left(2\dfrac{\omega-\omega_i}{\omega_{i-1}-\omega_i}\right)^K, & \dfrac{\omega_{i-1}+\omega_i}{2} \le \omega \le \omega_i \\ 1 - \dfrac{1}{2}\left(2\dfrac{\omega-\omega_i}{\omega_{i+1}-\omega_i}\right)^K, & \omega_i \le \omega \le \dfrac{\omega_i+\omega_{i+1}}{2} \\ \dfrac{1}{2}\left(2\dfrac{\omega-\omega_{i+1}}{\omega_i-\omega_{i+1}}\right)^K, & \dfrac{\omega_i+\omega_{i+1}}{2} \le \omega \le \omega_{i+1} \end{cases} \tag{15b}$$

$$w_N(\omega) = \begin{cases} \dfrac{1}{2}\left(2\dfrac{\omega-\omega_{N-1}}{\omega_N-\omega_{N-1}}\right)^K, & \omega_{N-1} \le \omega \le \dfrac{\omega_{N-1}+\omega_N}{2} \\ 1 - \dfrac{1}{2}\left(2\dfrac{\omega-\omega_N}{\omega_{N-1}-\omega_N}\right)^K, & \dfrac{\omega_{N-1}+\omega_N}{2} \le \omega \le \omega_N \\ 1, & \omega \ge \omega_N \end{cases} \tag{15c}$$

where exponent K is an integer. The window functions $w_i(\omega)$ with different values of K are illustrated in Fig. 3. In the numerical examples, K is set to 4. Since the static compact subcircuits are created by the micromodeling method in the concerned subfrequency band, they are a bandpass approximation of the original full-wave circuit model. Therefore, the role of the window function is to smooth and to interpolate the frequency response of the full-wave circuit model between subfrequency bands.

E. Stability, Causality, and Computational Overhead

The stability and causality of the simulated time-domain response are preserved by the passivity of the subcircuits and the transient analysis method used.

It has been theoretically proved in [28] that a circuit is passive when its resistance matrix, inductance matrix, and coefficients of potential matrix are positive semidefinite. The compact subcircuits obtained by the micromodeling method are guaranteed to be passive using the passivity enforcement

method in [28], which remedies the nonpassive elements directly by adding minor corrections on the elements. Such a passive system is guaranteed to be stable and causal, as theoretically proved in [33].

However, the stability and causality of a passive circuit may be violated in the numerical scheme of the time-domain simulation. For example, an inappropriate truncation of the frequency response for the convolution-based methods can lead to a noncausal frequency response [19], [20]. As demonstrated in [31], using the forward Euler differentiation formula in the transient analysis may cause numerical instability. To avoid the numerical instability and numerical causality problems, in the proposed method, the time-domain response of each subcircuit is obtained by the transient analysis using the trapezoidal differentiation formula that is adopted in SPICE. Equation (2) states that the output $\mathbf{y}_n$ at the nth time-step depends only on the signal $\mathbf{x}_{n-1}$, $\dot{\mathbf{x}}_{n-1}$, and $\mathbf{u}_n$ at the time-steps not larger than n. Therefore, the output response is causal. As stated in [31], the output response is also the numerical stable for passive circuits regardless of time-step when the trapezoidal differentiation formula is used. Since the simulated time-domain outputs of all the passive subcircuits are stable and causal, the sum of them is stable and causal.

The computational workload of the method is dominated by two processes: 1) deriving compact subcircuits using the micromodeling method, which can be executed by GPU and takes negligible portion of time when compared with that of the circuit simulation and 2) the transient analysis of all the subcircuits, which takes the major portion of time and can be accomplished by multiple CPUs in parallel. Using the micromodeling method, the original G-PEEC model with N nodes can be reduced to a compact subcircuit with only $N/10$ nodes. The computational overhead of deriving a compact subcircuit is $O(N^3)$ [27], which can be accelerated using the GPU parallel computation by tens of times [34], [35].

The major computation time is spent on the transient analysis of all the compact subcircuits, which is particularly dominating when processing a long sequence of input pulse for the eye-diagram calculation. If the time interval is constant, as shown in Section II, the most dominating operation in the transient analysis is the matrix multiplication. The computational overhead of one time-step calculation for a subcircuit with M nodes is $O(M^2)$. For K subcircuits and L time-steps, the total computational overhead is $O(KLM^2)$. When compared with the convolution-based methods, whose computation is dominated by matrix inversions with the computational overhead of $O(LM^3)$ for acquiring L samples of the frequency response. Considering the number of subcircuits K is in the order of tens whereas the number of samples L and the node number M are in the order of thousands, the computational efficiency of the proposed method is significantly high, not mentioning that the proposed method is free from the instability and noncausality problems.

The time-domain responses of different subcircuits can be computed independently by multiple CPUs. Let K be the number of subcircuits, T_0 be the time-domain simulation time of one subcircuit, and N be the number of CPUs, N subcircuits can be computed simultaneously. The total simulation time T can be estimated by

$$T = \begin{cases} \text{ceil}(K/N) \times T_0, & N < K \\ T_0, & N \geq K \end{cases} \tag{16}$$

where function ceil(x) maps x to the least integer greater than or equal to x.

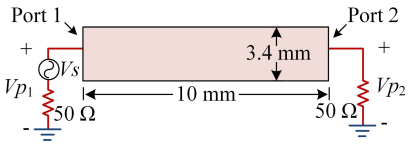

Fig. 4. Top view of the microstrip line.

V. Numerical Examples

Three numerical examples are provided to demonstrate the effectiveness, accuracy, and scalability of the proposed method. The first example is a short 50-Ω microstrip line, which is used to show how the Gibbs phenomenon can be eliminated. The second example demonstrates the accuracy of the transient response of the proposed method by analyzing a pulse signal passing through a dispersive meander line. The final example is the calculation of eye-diagrams of a multilayer multiport interconnection circuit, which shows the stability and causality of the proposed method.

As mentioned in Section IV-A, in the method of [32] and other convolution-based methods, the influence of the frequency response in the frequency band of $[-\infty, -\omega_N] \cup [\omega_N, +\infty]$ is omitted, which causes the Gibbs phenomenon in the transient analysis. In the numerical examples, the results by the method proposed in [32], which is called a frequency uncompensated subcircuit (FUS) method, are used for comparison purpose.

In all the numerical examples, the G-PEEC model with a mixed rectangular and triangular meshing scheme and the full-wave layered Green's functions are used. The CPU module used for all the examples is Intel i7 6700K with four cores, the clock speed of which is 3.4 GHz and arithmetic capability is 256 Gflops. The GPU module is Nvidia Geforce GTX 980 Ti with 2816 cores, the arithmetic capability of which is 5632 Gflops. The RAM size of the PC is 32 GB.

A. Short Microstrip Line Circuit

A short microstrip line whose substrate thickness is 1.5 mm and relative permittivity is 3.38 is shown in Fig. 4. The conductor thickness of the microstrip line is 10 μm, whose conductivity is 5.8×10^7 s $\cdot$ m^{-1}. The ground plane is treated as infinitely large in the G-PEEC model.

To show the significance of introducing $x_N(t)$ for alleviating the Gibbs phenomenon, the simulation results with and without the Nth subcircuit, which is the case in [32], are compared. The circuit is excited at port 1. The input signal V_s is a pulse function as shown in Fig. 5(a), whose pulsewidth is 1/2.4 ns. The total voltages at ports 1 and 2, namely, Vp_1 and Vp_2, respectively, are calculated using the proposed

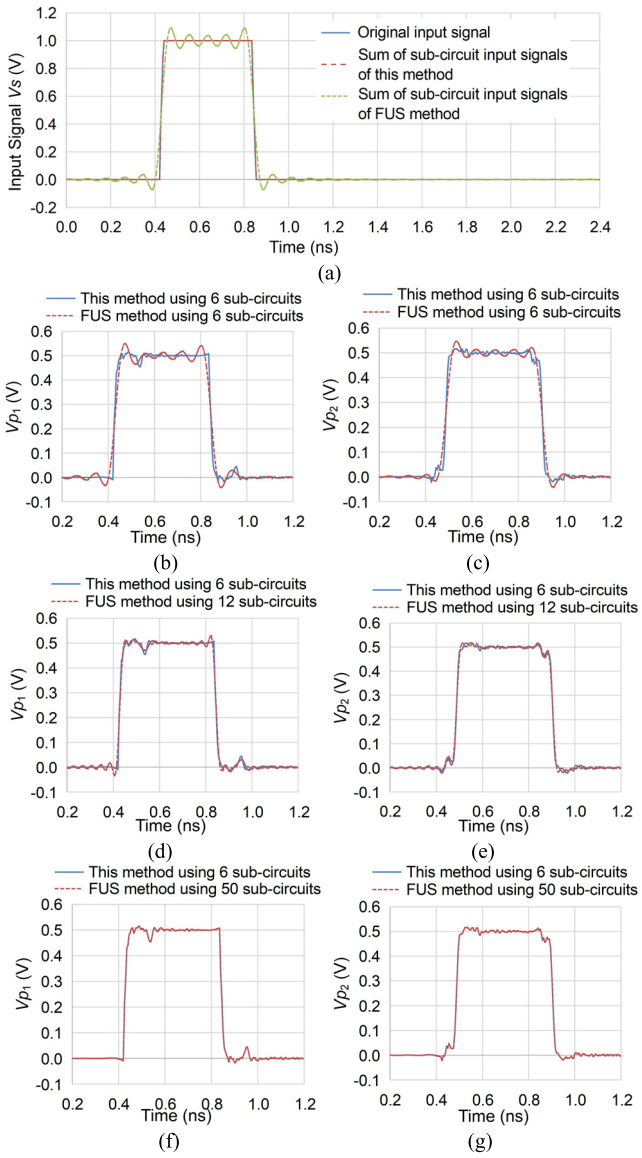

Fig. 5. Input signal and output response of the microstrip line simulated by this method using 6 subcircuits and the FUS method using different number of subcircuits. (a) Input signal. (b) Vp_1 by FUS method using 6 subcircuits. (c) Vp_2 by FUS method using 6 subcircuits. (d) Vp_1 by FUS method using 12 subcircuits. (e) Vp_2 by FUS method using 12 subcircuits. (f) Vp_1 by FUS method using 50 subcircuits. (g) Vp_2 by FUS method using 50 subcircuits.

method and the FUS method. In the proposed method, six subcircuits are sampled at frequencies of 0.1, 3, 6, 8, 10, and 12 GHz, respectively. Whereas in the FUS method, 6, 12, and 50 subcircuits are used, separately, to show the convergence.

First, the total input signals of the proposed method and FUS method using six subcircuits that are obtained by summarizing the input signals of the respective subcircuits are compared in Fig. 5(a), which shows that the total input signal of this method is the same as the original input signal V_s but that by the FUS method exhibits the Gibbs phenomena. As a result, the voltages Vp_1 and Vp_2 obtained by this method do not show obvious Gibbs phenomenon and those obtained by the FUS method have an obvious ripple as shown in Fig. 5(b) and (c).

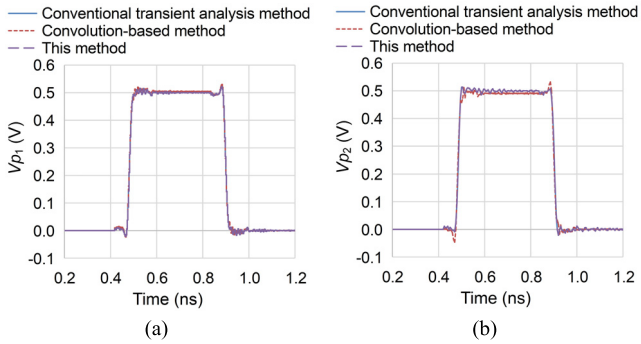

Fig. 6. Comparison of conventional transient analysis method, convolution-based method, and this method. (a) Output Vp_1. (b) Output Vp_2.

When the maximum sampling frequency and the number of subcircuits are increased for the FUS method, the bandwidth of the subcircuit input signals is increased, which will help decrease the Gibbs phenomena. For example, when the FUS method takes 12 subcircuits, and its maximum sampling frequency is increased from 12 to 25 GHz, the ripple of the output voltages decreases significantly as shown in Fig. 5(d) and (e). As shown in Fig. 5(f) and (g), when the number of subcircuits is increased to 50 with the maximum sampling frequency of 100 GHz, the ripple of the outputs converges and matches with those obtained by the proposed method with only six subcircuits, demonstrating that the proposed method is very effective in eliminating the Gibbs phenomenon.

In this example, the convolution-based method using IFFT is also studied for comparison purpose, in which the microstrip line is modeled by a quasi-static micromodeling circuit. In the setting of the convolution-based method, the cutoff frequency in generating the frequency response is 100 GHz. The time intervals for both the proposed and the convolution-based methods are set to 5 ps. The output signals Vp_1 and Vp_2 computed by both the methods are compared in Fig. 6. Because the quasi-static circuit consists of constant-valued *RLC* elements, its output response can be obtained accurately by conventional transient analysis method, which is used to validate the accuracy of the proposed method and the convolution-based method. The outputs obtained by the proposed method matches well with the conventional transient analysis method, which demonstrates that this method has good compatibility. However, the results obtained by the convolution-based method have a minor difference with the conventional transient analysis method, which may be caused by the inaccuracy of the impulse response introduced by the aliasing problem in IFFT.

B. Microstrip Meander Line Circuit

A microstrip meander line is considered in this example. The top view of the meander line is shown in Fig. 7. The substrate and the conductor are the same as those of the first example. The ground is treated as infinitely large in generating the full-wave G-PEEC model.

In simulating the time-domain responses, two kinds of subcircuits are adopted for the proposed method: a compact

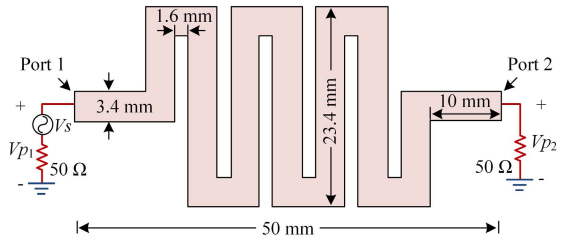

Fig. 7. Top view of the meander line.

TABLE I
COMPARISON OF DIRECT SUBCIRCUIT AND COMPACT SUBCIRCUIT

	Direct Sub-circuit	Compact Sub-circuit
No. of nodes	1092	152
No. of potors	1090	150
No. of capacitive couplings	593505	11175
No. of inductors	1959	292
No. of inductive couplings	1917861	42486
One sub-circuit generation time	20 sec	4 sec
Time-domain simulation time of a sub-circuit (5000 time-steps)	42 min 12 sec	35 sec

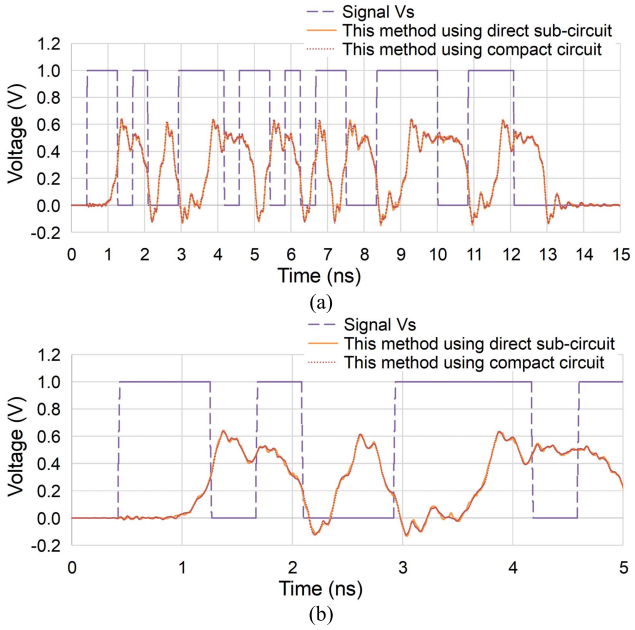

Fig. 8. Input signal V_S and time-domain response Vp_2 of the microstrip meander line circuit. (a) Source voltage V_s and Vp_2 simulated using compact subcircuits and direct subcircuits. (b) Zoomed-in view figure of (a).

subcircuit that is derived from the G-PEEC model using the micromodeling circuit and a direct subcircuit obtained directly from the G-PEEC model. The compact subcircuit contains 152 nodes, and the direct subcircuit contains 1092 nodes. To generate the compact subcircuit, the accuracy criterion δ_c is set to be 0.01. The input pulse with pulsewidth of 1/2.4 ns is shown in Fig. 8(a), which corresponds to the maximum subcircuit sampling frequency of 12 GHz. For a fair comparison, the direct subcircuits are sampled at the same frequency points as those for compact subcircuits. It is found that the variation in circuit elements in the direct subcircuit is much smaller than that of the compact subcircuits in the same subfrequency band. It is expected that the simulation result by the direct subcircuits is more accurate than that of the compact subcircuits. Therefore, the results obtained by the direct subcircuits can be used to validate the accuracy of the proposed method using the compact subcircuits. Nevertheless, the modeling time for one direct subcircuit and that for one compact subcircuit is 20 and 4 s, respectively. The details of the two kinds of subcircuits are compared in Table I.

As shown in Fig. 7, source V_s is applied at port 1 in series with a 50-Ω source resistance and a 50-Ω load resistance is used to terminate port 2. In the simulation, 15 subcircuits are used with sampling frequencies of 1, 2, 3, 4, 5, 6, 6.95, 7.8, 8.55, 9.25, 9.9, 10.5, 11.05, 11.55, and 12 GHz, respectively. As observed in Fig.8(a) and (b), the port voltages simulated using the compact subcircuits match well with those using the direct subcircuits. However, by adopting the compact subcircuit, the simulation time is reduced from 42 min 12 s to 35 s, which leads to nearly two orders of magnitude time-saving.

To validate the continuity of the simulated frequency-domain responses and the accuracy of the proposed method, the numerical results of $|S_{21}|$ obtained by the full-wave

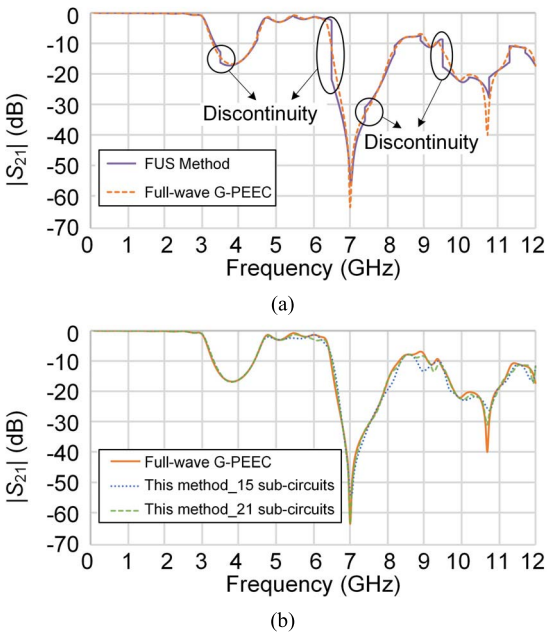

Fig. 9. Comparison of $|S_{21}|$ obtained by full-wave G-PEEC, FUS method, the method using 15 subcircuits, and the method using 21 subcircuits. (a) $|S_{21}|$ obtained by full-wave G-PEEC and FUS method. (b) $|S_{21}|$ obtained by full-wave G-PEEC, the method using 15 subcircuits, and the method using 21 subcircuits.

G-PEEC, the FUS method, the method using 15 subcircuits, and the method using 21 subcircuits are compared in Fig. 9. As shown in Fig. 9(a), the simulated $|S_{21}|$ obtained by the FUS method is discontinuous and the accuracy is poor. Using the proposed method, as shown in Fig. 9(b), the simulated $|S_{21}|$ is continuous. The simulated $|S_{21}|$ using 21 subcircuits is more accurate than that of using 15 subcircuits, demonstrating

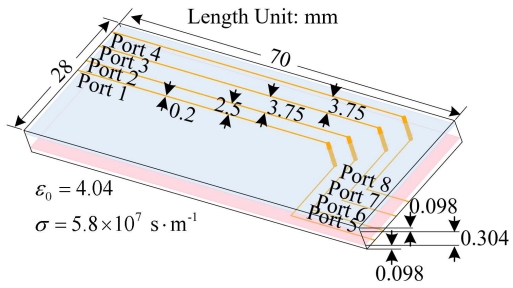

Fig. 10. Layout of a multilayer multiport interconnection circuit.

TABLE II
COMPARISON OF DIRECT SUBCIRCUIT AND COMPACT CIRCUIT

	Direct Sub-circuit	Compact Sub-circuit
No. of nodes	9785	1016
No. of potors	9769	1000
No. of capacitive couplings	47711796	499500
No. of inductors	18477	2158
No. of inductive couplings	170690625	2327403
One sub-circuit generation time	19 min 3 s	21 min 1 s
Eye-diagram simulation time of each sub-circuit	8463 min 44 s	40 min 41 s
Total eye-diagram simulation time using this method		569 min 34 s
Total eye-diagram simulation time using IFFT		1685 min 4 s

that the accuracy of this method depends on the number of subcircuits.

C. Multilayer Multiport Interconnection Circuit

The third example is a multilayer multiport interconnection circuit, which is used to show the efficiency of this method for computing eye-diagrams of a relatively large-scale interconnection circuit. As illustrated in Fig. 10, the circuit consists of four signal traces on the top and bottom layers, which are connected through holes. The overall dimensions of the circuit are $70 \times 28 \times 0.5$ mm^3. The conductor thickness is set to 10 μm with conductivity 5.8×10^7 s $\cdot$ m^{-1} in the G-PEEC model. The relative permittivity of the substrate is 4.04.

Similar to example II, the compact subcircuits that are derived from the G-PEEC model by the micromodeling method and direct subcircuits obtained from the G-PEEC model directly are compared to validate the accuracy of the proposed method. The compact subcircuit contains 1016 nodes, whereas the direct subcircuit contains 9785 nodes. In generating the compact subcircuit, the accuracy criterion δ_c is set to 0.01. For a fair comparison, the direct and compact subcircuits are sampled at the same frequency points. The details of the two subcircuits are listed in Table II.

The time-domain simulation of eye-diagrams is very time-consuming because a long PRBS is applied as the input signal. In this example, the 256-bit PRBS pulse signals are excited at ports 1 and 2, respectively, while the other ports are set as the output ports. The pulsewidth of the input signal is 1/2.4 ns, which leads to the maximum subcircuit sampling frequency of 12 GHz. To obtain reliable transient responses, 14 subcircuits are generated from the full-wave micromodeling

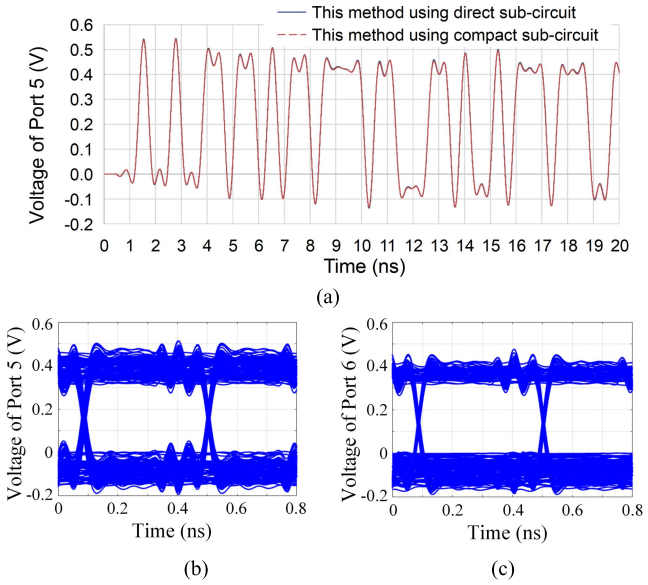

Fig. 11. Time-domain response of the interconnection circuit. (a) Transient response at port 5 of the first subcircuit. (b) Eye-diagram of output voltage at port 5. (c) Eye-diagram of output voltage at port 6.

circuit with sampling frequencies of 1, 2.8, 4.3, 5.45, 6.4, 7.25, 8.0, 8.7, 9.35, 9.95, 10.5, 11, 11.5, and 12 GHz. Because the simulation time using direct subcircuits is prohibitively long, only the output response of the first direct subcircuit is calculated and is compared with that using the compact subcircuit in Fig. 11(a), showing excellent agreement. The simulation time for using one direct subcircuit and one compact subcircuit is 8463 min 44 s and 40 min 41, respectively. The eye-diagrams of output voltages at ports 5 and 6 simulated by the proposed method are shown in Fig. 11(b) and (c). It can be seen that the proposed method is stable and importantly suitable for a large-scale interconnection problem.

The proposed method computes the time-domain response of compact subcircuits using the transient analysis method [30] in time-domain directly, which can achieve high efficiency when compared with the IFFT method. To demonstrate the point, the eye-diagram of the circuit is also computed by the IFFT method using the same compact subcircuits. According to Nyquist sampling theorem, 21 335 frequency response samples are needed by the IFFT method. As a result, the total eye-diagram simulation time using the IFFT method is 1685 min 4 s, whereas 569 min 34 s is taken using the proposed method.

The simulation time for the eye-diagram using the compact subcircuits is less than that of using the direct subcircuits by more than two orders of magnitude and is much less than that of the IFFT method using the same compact subcircuits, justifying that the micromodeling circuit method can significantly speed up the SI analysis without sacrificing the accuracy and stability.

VI. CONCLUSION

This article presents a transient analysis method of a full-wave G-PEEC model for high-speed packaging and

interconnection problems. In the proposed transient analysis method, a full-wave circuit model whose elements are frequency variant is decomposed into a number of static, passive, and compact subcircuits that are derived from the G-PEEC model by the micromodeling method. Therefore, the transient response of a full-wave circuit model can easily be obtained by summing up the individual response of each compact subcircuit. The output response of a passive subcircuit can be simulated by a traditional transient analysis tool. By introducing a frequency compensation strategy and window functions, the proposed method does not suffer from the truncation error of an input signal or a frequency response of a finite frequency band, nor the Gibbs phenomena. By adopting the compact subcircuits, a transient simulation can not only be accelerated by two orders of magnitude when compared with the direct use of the full-wave G-PEEC model but also be with guaranteed stability and causality. Three numerical examples are given to demonstrate the efficiency, accuracy, and simplicity of the proposed method. The comparison is made between the proposed method using the compact subcircuits, the proposed method using the direct subcircuits, and a convolution-based method, showing the superiority of the proposed method and a high potential for efficient simulation of the large-scale high-speed interconnection and packaging problems.

REFERENCES

[1] W. T. Beyene, X. Yuan, N. Cheng, and H. Shi, "Design, modeling, and hardware correlation of a 3.2 Gb/s/pair memory channel," *IEEE Trans. Adv. Packag.*, vol. 27, no. 1, pp. 34–44, Feb. 2004.

[2] T. J. Brazil, "Causal-convolution—A new method for the transient analysis of linear systems at microwave frequencies," *IEEE Trans. Microw. Theory Techn.*, vol. 43, no. 2, pp. 315–323, Feb. 1995.

[3] S. N. Lalgudi, A. E. Engin, G. Casinovi, and M. Swaminathan, "Accurate transient simulation of interconnects characterized by band-limited data with propagation delay enforcement in a modified nodal analysis framework," *IEEE Trans. Electromagn. Compat.*, vol. 50, no. 3, pp. 715–729, Aug. 2008.

[4] S. Kapur, D. E. Long, and J. Roychowdhury, "Efficient time-domain simulation of frequency-dependent elements," in *Proc. ICCAD*, San Jose, CA, USA, Nov. 1996, pp. 569–573.

[5] P. A. Perry and T. J. Brazil, "Forcing causality on *S*-parameter data using the Hilbert transform," *IEEE Microw. Guided Wave Lett.*, vol. 8, no. 11, pp. 378–380, Nov. 1998.

[6] P. Triverio and S. Grivet-Talocia, "Causality-constrained interpolation of tabulated frequency responses," in *Proc. IEEE Elect. Performane Electron. Packag.*, Scottsdale, AZ, USA, Oct. 2006, pp. 181–184.

[7] J. Becerra, F. Vega, and F. Rachidi, "Extrapolation of a truncated spectrum with Hilbert transform for obtaining causal impulse responses," *IEEE Trans. Electromagn. Compat.*, vol. 59, no. 2, pp. 454–460, Apr. 2017.

[8] F. Rao, "Optimization of spectrum extrapolation for causal impulse response calculation using the Hilbert transform," U.S Patent 7962541 B2, Jun. 14, 2011.

[9] S. Luo and Z. Chen, "Iterative methods for extracting causal time-domain parameters," *IEEE Trans. Microw. Theory Techn.*, vol. 53, no. 3, pp. 969–976, Mar. 2005.

[10] S. M. Narayana *et al.*, "Interpolation/extrapolation of frequency domain responses using the Hilbert transform," *IEEE Trans. Microw. Theory Techn.*, vol. 44, no. 10, pp. 1621–1627, Oct. 1996.

[11] W. T. Beyene and C. Yuan, "An accurate transient analysis of high-speed package interconnects using convolution technique," *Analog Integr. Circuits Signal Process.*, vol. 35, pp. 107–120, May 2003.

[12] B. Gustavsen and A. Semlyen, "Rational approximation of frequency domain responses by vector fitting," *IEEE Trans. Power Del.*, vol. 14, no. 3, pp. 1052–1061, Jul. 1999.

[13] B. Gustavsen, "Improving the pole relocating properties of vector fitting," *IEEE Trans. Power Del.*, vol. 21, no. 3, pp. 1587–1592, Jul. 2006.

[14] Y. S. Mekonnen and J. E. Schutt-Aine, "Broadband macromodeling of sampled frequency data using z-domain vector-fitting method," in *Proc. 11th IEEE Workshop Signal Propag. Interconnects*, Genova, Italy, May 2007, pp. 45–48.

[15] E.-P. Li, E.-X. Liu, L.-W. Li, and M.-S. Leong, "A coupled efficient and systematic full-wave time-domain macromodeling and circuit simulation method for signal integrity analysis of high-speed interconnects," *IEEE Trans. Adv. Packag.*, vol. 27, no. 1, pp. 213–223, Feb. 2004.

[16] L. T. Pillage and R. A. Rohrer, "Asymptotic waveform evaluation for timing analysis," *IEEE Trans. Comput.-Aided Design Integr. Circuits Syst.*, vol. 9, no. 4, pp. 352–366, Apr. 1990.

[17] J. E. Bracken, V. Raghavan, and R. A. Rohrer, "Interconnect simulation with asymptotic waveform evaluation (AWE)," *IEEE Trans. Circuits Syst. I, Fundam. Theory Appl.*, vol. 39, no. 11, pp. 869–878, Nov. 1992.

[18] K. S. Oh, "Accurate transient simulation of transmission lines with the skin effect," *IEEE Trans. Comput.-Aided Design Integr.*, vol. 19, no. 3, pp. 389–396, Mar. 2000.

[19] S. Roy and A. Dounavis, "Transient simulation of distributed networks using delay extraction based numerical convolution," *IEEE Trans. Comput.-Aided Design Integr. Circuits Syst.*, vol. 30, no. 3, pp. 364–373, Mar. 2011.

[20] R. Mandrekar, K. Srinivasan, E. Engin, and M. Swaminathan, "Causal transient simulation of passive networks with fast convolution," in *Proc. 10th IEEE Workshop Signal Propag. Interconnects*, May 2006, pp. 61–64.

[21] M. Tsuk and S. Lalgudi, "Least squares convolution: A method to improve the fidelity of convolution in transient circuit simulation," in *Proc. IEEE Conf. Electr. Perform. Electron. Packag. Syst.*, Portland, OR, USA, Oct. 2009, pp. 73–76.

[22] S. Lefteriu and A. C. Antoulas, "On the convergence of the vector-fitting algorithm," *IEEE Trans. Microw. Theory Techn.*, vol. 61, no. 4, pp. 1435–1443, Apr. 2013.

[23] B. Gustavsen and A. Semlyen, "Fast passivity assessment for *S*-parameter rational models via a half-size test matrix," *IEEE Trans. Microw. Theory Techn.*, vol. 56, no. 12, pp. 2701–2708, Dec. 2008.

[24] L. K. Yeung and K.-L. Wu, "Generalized partial element equivalent circuit (PEEC) modeling with radiation effect," *IEEE Trans. Microw. Theory Techn.*, vol. 59, no. 10, pp. 2377–2384, Oct. 2011.

[25] L. K. Yeung and K.-L. Wu, "PEEC modeling of radiation problems for microstrip structures," *IEEE Trans. Antennas Propag.*, vol. 61, no. 7, pp. 3648–3655, Jul. 2013.

[26] C.-C. Chou, W.-C. Lee, and T.-L. Wu, "A rigorous proof on the radiation resistance in generalized PEEC model," *IEEE Trans. Microw. Theory Techn.*, vol. 64, no. 12, pp. 4091–4097, Dec. 2016.

[27] Y. Dou and K.-L. Wu, "A passive full-wave micromodeling circuit for packaging and interconnection problems," *IEEE Trans. Microw. Theory Techn.*, vol. 67, no. 6, pp. 2197–2207, Jun. 2019.

[28] Y. Dou and K.-L. Wu, "A passive PEEC-based micromodeling circuit for high-speed interconnection problems," *IEEE Trans. Microw. Theory Techn.*, vol. 66, no. 3, pp. 1201–1214, Mar. 2018.

[29] Y. Dou and K.-L. Wu, "Direct mesh-based model order reduction of PEEC model for quasi-static circuit problems," *IEEE Trans. Microw. Theory Techn.*, vol. 64, no. 8, pp. 2409–2422, Aug. 2016.

[30] C.-W. Ho, A. Ruehli, and P. Brennan, "The modified nodal approach to network analysis," *IEEE Trans. Circuits Syst.*, vol. CAS-22, no. 6, pp. 504–509, Jun. 1975.

[31] K. G. Nichols, T. J. Kazmierski, M. Zwolinski, and A. D. Brown, "Overview of SPICE-like circuit simulation algorithms," *IEE Proc.-Circuits, Devices Syst.*, vol. 141, no. 4, pp. 242–250, Aug. 1994.

[32] Y. Dou, L. K. Yeung, and K.-L. Wu, "Time-domain analysis of circuits with frequency-dependent elements using a SPICE-like solver," in *Proc. IEEE Elect. Design Adv. Packag. Syst. Symp.*, Nara, Japan, Dec. 2013, pp. 193–196.

[33] S. Grivet-Talocia and B. Gustavsen, "Linear time-invariant circuits and systems," in *Passive Macromodeling, Theory Applications*, 1st ed. Hoboken, NJ, USA: Wiley, 2016, pp. 26–27.

[34] Y. Dou and K.-L. Wu, "Acceleration of a physically derived micro-modeling circuit for packaging problems using graphics processing units," in *IEEE MTT-S Int. Microw. Symp. Dig.*, Honolulu, HI, USA, Jun. 2017, pp. 1638–1640.

[35] Y. Dou and K.-L. Wu, "Acceleration of parallel computation for derived micro-modeling circuit by exploiting GPU memory bandwidth limit," in *Proc. IEEE Int. Conf. NEMO*, Seville, Spain, May 2017, pp. 146–148.

[36] A. V. Oppenheim, A. S. Willsky, and S. H. Naab, "Fourier analysis for continuous-time signals and systems," in *Signals Systems*, 2nd ed. London, U.K.: Pearson, 1997, ch. 4, pp. 194–195.

Yuhang Dou (S'13) received the B.S. degree in electronic engineering from the Nanjing University of Science and Technology, Nanjing, China, in 2012. She is currently pursuing the Ph.D. degree at The Chinese University of Hong Kong, Hong Kong.

Her current research interests include physics-based circuit-domain modeling methods for radiation problems and signal integrity (SI) analysis of high-speed large-scale interconnection and packaging problems.

Ms. Dou was a recipient of Fist Runner Up Awards of both the 2015 and 2018 IEEE Hong Kong AP/MTT Postgraduate Conference.

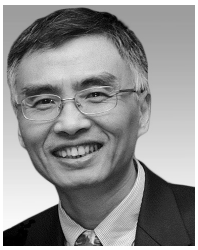

Ke-Li Wu (M'90–SM'96–F'11) received the B.S. and M.Eng. degrees from the Nanjing University of Science and Technology, Nanjing, China, in 1982 and 1985, respectively, and the Ph.D. degree from Laval University, Quebec, QC, Canada, in 1989.

From 1989 to 1993, he was a Research Engineer with McMaster University, Hamilton, ON, Canada. In 1993, he joined the Corporate Research and Development Division, Honeywell Aerospace, Cambridge, ON, Canada, where he was a Principal Member of Technical Staff. Since 1999, he has been with The Chinese University of Hong Kong, Hong Kong, where he is currently a Professor and the Director of the Radiofrequency Radiation Research Laboratory. His current research interests include EM-based circuit domain modeling of high-speed interconnections, robot automatic tuning of microwave filters, decoupling techniques of MIMO antennas, and Internet-of-Things technologies.

Dr. Wu is a member of the IEEE MTT-8 Subcommittee. He serves as a TPC member for many prestigious international conferences. He was a recipient of the 1998 COM DEV Achievement Award and the Asia–Pacific Microwave Conference Prize twice in 2008 and 2012, respectively. From 2006 to 2009, he was an Associate Editor of the IEEE TRANSACTIONS ON MICROWAVE THEORY AND TECHNIQUES.